ELSEVIER

Polymer 41 (2000) 9205–9217

polymer

www.elsevier.nl/locate/polymer

Orientation characteristics of LLDPE blown films and their implications on Elmendorf tear performance

R.K. Krishnaswamy*, A.M. Sukhadia

Phillips Petroleum Company, 94-G Phillips Research Center, Bartlesville, OK 74004, USA

Received 26 October 1999; received in revised form 4 January 2000; accepted 11 January 2000

Abstract

The orientation features of several linear low-density polyethylene (LLDPE) blown films were characterized and significant insights into the morphological origin of Elmendorf tear resistance were developed. The orientation features of all the LLDPE blown films investigated were described in terms of the Keller–Machin "row" structure. The machine direction (MD) tear resistance was observed to be higher when the non-crystalline chains were closer to equi-biaxial in the plane of the film. Further, the transverse direction (TD) tear resistance was observed to be high when the crystalline lamellae were minimally curved and oriented closer to the film TD. These results indicated that deformations in the interlamellar region and the stresses borne along the lamellar long axes play important roles in distinguishing the MD and TD tear resistances, respectively, of LLDPE blown films.

Keywords: Polyethylene; Linear low-density polyethylene; Blown films

1. Introduction

Close to five million metric tons of polyethylene are converted into film products in the USA every year. In fact, while 50% of all polyethylene (linear low-density polyethylene or LLDPE; low-density polyethylene or LDPE; high-density polyethylene or HDPE) is consumed in film applications, close to 90% of all LLDPE and LDPE is consumed in film applications [1,2]. Packaging applications dominate utilization of polyethylene film not only in the American, but also in European and Asian markets. Some examples of packaging applications include food packaging, trash and can-liners, shrink film, stretch film, and merchandise packaging. Packaging films are required to possess high resistance to tear propagation in most applications. Despite the commercial significance of polyethylenes in blown and cast film applications, a clear understanding of the morphological features that dictate their performance is still lacking. This is especially true for blown film tear properties, as there are no published studies that document in detail the morphological features associated with blown film tear propagation. This puts a serious damper on resin development efforts, especially in the development of resins with superior blown film tear resistance performance.

It is recognized that molecular orientation largely dictates the performance of blown films in their intended application. The orientation features of various LLDPE blown films have been characterized previously. However, very little has been achieved in terms of relating molecular orientation to tear performance. In this investigation, the biaxial orientation features in the crystalline and non-crystalline phases of various LLDPE blown films have been characterized. Specifically, twelve different LLDPE-type resins (density $\approx 0.920 g\ cm^{-3}$) that encompass those polymerized using Ziegler–Natta, metallocene and chromium oxide type catalysts were investigated. Further, the influence of process extension rate on the blown film tear performance of select LLDPE resins was also considered. This report is thus a summary of the process and morphology related factors that influence the tear performance of LLDPE blown films, with all tear properties measured using an Elmendorf tear test. For purposes of consistency, all LLDPE resins considered for this study were of a nominal $0.920\ g\ cm^{-3}$ density.

2. Background on solid-state deformation of polyethylene

Most performance measures of blown films involve mechanical destruction of the specimen. Therefore, if the morphological origin of blown film performance is of interest, it is important to understand the structural changes that

* Corresponding author. Tel.: + 1-918-661-9906.
E-mail address: rkkrish@ppco.com (R.K. Krishnaswamy).

0032-3861/00/$ - see front matter
PII: S0032-3861(00)00136-1

undergo when polyethylene is mechanically deformed. Therefore, in this section, previous research on the structural changes that have been identified when both unoriented and oriented polyethylene specimens were deformed under controlled conditions will be summarized.

The deformation of polyethylene and the associated morphological changes have been reviewed [3–8]. Most of the prior research has involved controlled deformation (usually in the tensile and compressive modes) of unoriented and oriented polyethylene specimens. This has been an area of interest to the academic and industrial communities largely due to the solid state processing of various polymers, such as ultra-high modulus polyethylene fibers and biaxially oriented polypropylene. While solid state deformation of polyethylene (and other polymers) has tremendous commercial significance, our interests lie in using the knowledge gained in this field to help understand the morphological origin of blown film tear performance. After all, tear testing involves solid state deformation of film specimens. Further, it is recognized that substantial stretching of the film specimen occurs prior to tear propagation in an Elmendorf tear test (ASTM D-1922).

A general classification of the microstructural deformation mechanisms known to be operative during controlled deformation of polyethylene is shown below [3]:

- Deformation of the non-crystalline (amorphous) phase
  - Interlamellar shear
  - Interlamellar separation
  - Lamellar rotation
- Deformation of the crystalline phase
  - Crystallographic slip (chain slip, transverse slip, dislocation generation)
  - Mechanical twinning and stress-induced martensitic transformation
  - Decrystallization and recrystallization

Excellent illustrative representations of these deformation mechanisms are documented in a recent review [3]. When polyethylene is deformed at room temperature, the non-crystalline phase being above its glass transition temperature tends to deform first and at low-strain levels. *Interlamellar shear* involves shearing of the non-crystalline chains between adjacent lamellae, with the shear direction being parallel to the lamellar surface. Interlamellar shear deformation is likely to involve taut "tie-molecules" and is dominant when lamellar normals (and the taut tie-molecules) make an angle of 45° with respect to the deformation/load direction [3,7,8]. *Interlamellar separation* involves a change in the distance between adjacent lamellae as measurable by small-angle X-ray scattering (SAXS). This deformation mechanism is believed to depend on the number and density of taut tie-molecules between adjacent lamellae and the lateral dimension of the lamellae [3,7,8]. Like interlamellar shear, interlamellar separation is also largely recoverable; the reversibility of these deformation mechanisms is due to the rubbery nature of the non-crystalline chain segments at room temperature. Interlamellar separation is dominant when lamellar normals are along the deformation/load direction [3,7,8]. *Lamellar rotation* is a mechanism that allows the structure to accommodate deformations occurring in the non-crystalline phase, such as interlamellar shear and separation. Lamellar rotation has been observed to occur alongside interlamellar shear and interlamellar separation in oriented LDPE films [7,8]. Therefore, lamellar rotation is not considered to be an independent deformation mechanism, but one that facilitates other deformations in the non-crystalline phase.

Slip is the *dominant* mode of plastic deformation in polymer crystals [3]. The presence of dislocations in polymer crystals is well recognized. When the resolved shear stress on a slip plane in a given slip direction is greater than a critical value, movement of dislocations can lead to relative translation of the two parts of the crystal that are separated by the slip plane. Deformation by crystallographic slip is usually governed by the resistance to the motion of dislocations on the slip planes [3]. The long chain nature of polymer molecules requires that the most preferred slip plane in polymer crystals contains the molecular chain thus confining slip along planes of the (*hk*0) type for polyethylene crystals; this is referred to as *chain slip*. Also, chain slip does not lead to distortion of simple unit cells such as the orthorhombic unit cell of polyethylene [3]. Further, post-yield deformation of polyethylene also involves certain decrystallization processes such as break-up of lamellae, chain pull-out along the lamellar long axis and so on.

3. Experimental section

All of the film blowing was carried out using a 38 mm diameter single screw Davis Standard extruder (L/D = 24; 2.2:1 compression ratio), which is fitted with a barrier screw with a Maddock mixing section at the end. Three sets of blown films were considered for this study and they are listed as SERIES-1 to SERIES-3 (details follow in Section 4). A 5.1 cm diameter Sano film die equipped with a single-lip air ring was employed for SERIES-1, and a 10.2 cm diameter Sano film die equipped with a dual-lip air ring was employed for SERIES-2 and SERIES-3. For SERIES-2 and SERIES-3, extruder and die temperatures were set to 190°C and the die-gap was 1.52 mm. For SERIES-3 films, the blow-up ratio was 2.5, the die gap was 1.52 mm and the extrusion rate was 27 kg h^{-1}.

All rheological tests were carried out on compression molded disks of the polymers in a Rheometrics RMS-800 rheometer using parallel plate geometry. Small strain (10%) dynamic mechanical experiments were performed at 190°C in a nitrogen atmosphere which yielded complex viscosity data as a function of imposed oscillatory frequency ($|\eta^*|$ vs. ω). Upon sample loading and thermal equilibration in the rheometer, the specimen disks were squeezed

Table 1
Description of the LLDPE resins used in this study. Molecular weight data are based on SEC measurements. Melt rheological characteristics are described in terms of the CY parameters calculated from torsional oscillatory measurements at 190°C. MI: melt index in dg min. Density: pellet density in g cc^{-1}. M_w: weight-average molecular weight in 10^3 g mol^{-1}. M_n: number-average molecular weight in 10^3 g mol^{-1}. M_w/M_n: molar mass distribution breadth index. M_z: z-average molecular weight in 10^3 g mol^{-1}. η_0: zero-shear viscosity at 190°C (Pa s). τ_η: C–Y viscous relaxation time at 190°C (s). a: rheological breadth parameter at 190°C

Resin	MI	Density	M_w	M_n	M_w/M_n	M_z	η_0	τ_η	a
LLDPE-1	0.9	0.921	119	22	7.1	532	1.75E + 04	0.032	0.36
LLDPE-2	0.8	0.923	144	20	7.1	912	3.17E + 04	0.046	0.27
LLDPE-3	0.5	0.919	135	29	4.7	542	2.86E + 04	0.052	0.36
LLDPE-4	1.0	0.920	105	27	4.0	410	1.04E + 04	0.026	0.41
LLDPE-5	1.0	0.918	105	46	2.3	207	8.81E + 03	0.015	0.57
LLDPE-6	0.9	0.921	108	31	3.4	284	1.08E + 04	0.023	0.40
LLDPE-7	0.2	0.922	208	11	18.9	2244	4.70E + 05	1.270	0.19
LLDPE-8	1.0	0.917	100	43	2.3	203	7.60E + 03	0.017	0.69
LLDPE-9	0.8	0.917	106	26	4.1	326	1.31E + 04	0.026	0.41
LLDPE-10	1.0	0.921	117	29	4.1	421	1.24E + 04	0.025	0.43
LLDPE-11	1.0	0.920	120	28	4.2	447	1.34E + 04	0.027	0.42
LLDPE-12	1.0	0.919	118	27	4.4	464	1.53E + 04	0.028	0.37

between the parallel plates to 1.6 mm thickness and the excess was trimmed prior to the actual test.

Molecular weight data were obtained using a Waters 150 CV Plus Gel Permeation Chromatograph using trichlorobenzene as the solvent with a flow rate of 1 ml min^{-1} at a temperature of 140°C. An injection volume of 220 μl was used with a nominal polymer concentration of 5 mg/3.5 ml of solvent (at room temperature). Parameter values used in the Mark–Houwink equation ($[\eta] = KM^a$) for polyethylene were $K = 39.5\ (10^{-3})$ ml g^{-1} and $a = 0.726$.

The Elmendorf tear properties of all blown films were measured according to ASTM D-1922, using a TMI Universal Tear Tester. Tensile tests were performed using an Instron Universal Test System, using a specimen length of 5.1 cm and a displacement rate of 51 cm min^{-1}. IR absorbance data (used to determine the biaxial orientation factors of the crystalline phase) were obtained using a FTS-40 Bio-Rad Spectrometer; spectra were obtained in the 400–4000 cm^{-1} range, with a resolution of 2 cm^{-1}. A nitrogen purge was used and all the IR scans were corrected for baseline effects. Data were collected with the incident IR radiation polarized parallel and perpendicular to the blown film MD. The IR absorbances of particular interest were those at 719 and 730 cm^{-1}. Details regarding how these absorbances were used in conjunction with the Beer–Lambert law to calculate the White–Spruiell biaxial orientation factors are documented elsewhere [9]. For blown film birefringence data, refractive index measurements along the film MD, TD, and normal direction (ND) were obtained using a Metricon Prism Coupler instrument equipped with the 200-P-1 prism ($n < 1.8$). The resolution (in refractive index measurements) of the Metricon Prism Coupler is of the order 0.0001.

All wide-angle X-ray scattering (WAXS) patterns and transmission electron miscoscopy (TEM) data were obtained through the courtesy of Prof. Garth Wilkes at Virginia Tech. All the WAXS patterns were performed utilizing a Philips tabletop X-ray generator (model PW1720) with CuKα irradiation ($\lambda = 0.154$ nm) and equipped with a standard vacuum-sealed photographic pinhole camera. The instrument was operated at 40 kV and 50 mA. All TEM images were taken with a Philips EM-420 scanning transmission electron microscope operated in the transmission mode at 100 kV. Samples were prepared by staining with chlorosulfonic acid.

4. Results

4.1. LLDPE resin and film processing characteristics

Table 1 lists the molecular weight and melt rheological attributes of each LLDPE resin considered for this study. All the resins considered here are of comparable density (~0.920 g cm^{-3}). The resin set includes polyethylenes made using metallocene catalysts, chromium oxide catalyst and conventional Ziegler–Natta type catalysts. The molecular weight data are based on size exclusion chromatographic (SEC) measurements. While the densities of all the LLDPE resins are approximately 0.920 g cm^{-3}, the weight average molecular weight ranges between 100,000 and 200,000 g mol^{-1} and the breadth in molecular weight distribution ranges between 2.3 and 19.0. In general, the three classes of LLDPEs in this set of polymers can be distinguished by their molecular weights and molecular weight distribution. Within the set of polymers considered, metallocene catalyzed LLDPEs display narrow molecular weight distributions (MWD < 3.5), chromium oxide catalyzed LLDPEs display very broad molecular weight distributions (MWD > 15) and Ziegler–Natta catalyzed LLDPEs display intermediate molecular weight distributions (3.6 < MWD < 8).

The melt rheology of these resins were characterized by performing dynamic oscillatory measurements at 190°C and

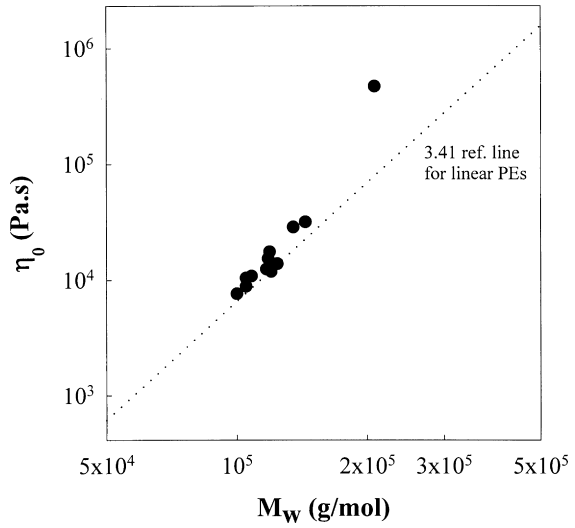

Fig. 1. Plot of zero shear viscosity (η_0) versus weight average molecular weight (M_w) for the LLDPE resins considered. The dotted line (slope of 3.41) corresponds to the anticipated η_0 for linear molecules of the same M_w.

the resulting data ($|\eta^*|$ vs. ω) were fitted to the Carreau–Yasuda (CY) model:

$$|\eta^*| = \eta_0[1 + (\tau_\eta\omega)^a]^{n-1/a} \quad (1)$$

where, $|\eta^*(\omega)|$ is the scalar magnitude of the complex viscosity, η_0 the zero-shear viscosity, ω the angular frequency, τ_η the characteristic viscous relaxation time, a is a parameter that is inversely related to the breadth of the transition from Newtonian to power-law behavior, and n fixes the final slope of the viscosity at high frequencies. The CY parameters of all the above LLDPE resins are also listed in Table 1. The CY model has been used successfully within Phillips Petroleum to describe the shear rheology of polyethylene melts. Details of the data treatment and the significance of the CY parameters are described elsewhere [10]. In Fig. 1, a log–log plot of zero shear viscosity (η_0) versus weight average molecular weight (M_w) is shown for the twelve LLDPE resins considered here. Also shown in the same plot is a straight line with a slope of 3.41 that corresponds to the anticipated η_0 for linear molecules of the same molecular weight (M_w). As evident in Fig. 1, all but one of the LLDPEs considered fall within the statistical limits of strictly "linear" polyethylenes with η_0 displaying a power-law dependence on M_w at an index of 3.41. This is consistent with the Arnett and Thomas result for linear hydrogenated polybutadienes [11]. LLDPE-7 displays a significant offset from this linear dependence indicating the presence of rheologically significant long branches. The long chain branching content in polyethylenes can now be quantified as described by Janzen and Colby [12]. As per their analysis, even LLDPE-7 consists of less than 10 rheologically significant long branches per million carbon atoms in the polymer. This is orders of magnitude lower than the long chain branch density in LDPEs (polymerized in high-pressure processes) which are typically considered as being highly branched polyethylenes.

Table 3
Blown film process conditions for SERIES-2 films: a process study using LLDPE-4

Blow-up ratio	Extrusion rate (kg/h)	Draw-down ratio	
25 and 50 μm thick films		25 (μm)	50 (μm)
1.8	27.3	34	17
3.0	27.3	20	10
2.1	13.6	29	15
3.0	13.6	34	17

In this paper, results from three different studies are summarized with an emphasis on blown film tear properties. The following (labeled SERIES-1 to SERIES-3) are the studies considered:

- *SERIES-1:* The influence of process parameters on the tear properties of LLDPE blown films was investigated. In this series, LLDPE-7 was blown into 25 μm thick film at several "high-stalk" or "HDPE" process conditions [13]. The details of the process variables are listed in Table 2 and the process equipment employed are stated in Section 3.
- *SERIES-2:* The influence of process parameters on the tear properties of LLDPE blown films was investigated. In this series, LLDPE-4 was blown into 25 and 50 μm thick films at different blow-up ratios and extrusion rates using the "in-pocket" or "LLDPE" bubble configuration [13]. The details of the process variables are listed in Table 3 and the process equipment employed are stated in Section 3.
- *SERIES-3:* In this series, the processing conditions were

Table 2
Blown film process conditions for SERIES-1 blown films: a process study on LLDPE-7

SERIES-1 Film #	Die gap (mm)	Extrusion temperature (°C)	Extrusion rate (kg/h)	Frost line height (mm)	Blow-up ratio	Draw-down ratio
LLDPE-7-1	0.9	221	18.7	381	4	9
LLDPE-7-2	0.9	250	7.3	229	2	18
LLDPE-7-3	0.9	250	7.0	762	6	6
LLDPE-7-4	0.9	200	19.0	762	6	6
LLDPE-7-5	0.9	250	19.8	762	6	6
LLDPE-7-6	0.9	250	16.5	229	6	6
LLDPE-7-7	1.9	250	6.9	279	2	38

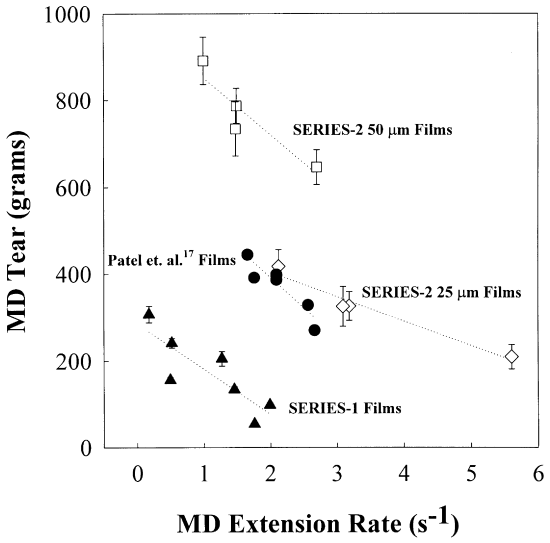

Fig. 2. LLDPE blown film MD tear resistance plotted as a function of MD extension rate for SERIES-1 and SERIES-2 films.

kept constant and all the LLDPEs listed in Table 1 were blown into 25 μm thick films using the "in-pocket" or "LLDPE" bubble configuration [13]. Specifically, a blow-up ratio of 2.5, draw-down ratio of 24, die-gap of 1.52 mm, extrusion rate of 27 kg h^{-1}, and extrusion temperature of 190°C were employed. These process conditions (described in Section 3), by means of scale-up strategy developed previously [14], are believed to scale closely to typical commercial scale processing of similar resins.

4.2. Influence of process extension rate on LLDPE blown film tear resistance

Momentum balance of the blown film process leads to an equation for the extension rate profile along the bubble as a function of distance from the die exit. The extension rate along the film MD is expressed by Ghaneh-Fard et al. [15,16] as follows:

$$\dot{\varepsilon}_{MD} = 2\frac{dv_z}{dz} + 2v_z\left(\frac{dr}{dz}\right)\left(\frac{d\theta}{dz}\right) \quad (2)$$

where v_z is the axial film velocity, r the bubble radius, and θ the bubble inflation angle. The machine direction extension rate at the frost line can thus be approximated as follows:

$$\dot{\varepsilon}_{MD} \approx 2\frac{v_{FL} - v_{die}}{FLH} \quad (3)$$

where the subscripts 'FL' and 'die' indicate frost-line and die exit, respectively, and 'FLH' is the frost-line height.

In SERIES-1, LLDPE-7 was blown under high-stalk conditions at different extrusion rates, extrusion temperatures, frost-line heights, blow-up ratios and die gaps (Table 2). Clearly, the MD tear resistance of the resulting films is a strong function of the process conditions employed. In Fig. 2, the MD tear resistance of the SERIES-1 blown films is plotted as a function of the average MD extension rate (as estimated using Eq. (3)). The MD tear of the blown films display a strong sensitivity to the extension rate along the MD, with the films processed at low MD extension rates displaying higher MD tear resistance.

SERIES-2 corresponds to films blown at various conditions using LLDPE-4. The MD tear of these 25 and 50 μm thick blown films are also plotted as a function of the MD extension rate in Fig. 2. For both the 25 and 50 μm thick films, processing at lower extension rates resulted in higher MD tear resistance. This is consistent with the results observed for SERIES-1 films. Also, when the MD tear of the 50 μm thick films are divided by two and compared to the MD tear of the 25 μm thick films at corresponding blow-up ratios and extrusion rates, these normalized MD tear numbers are systematically higher than those measured for the 25 μm thick films. This is again due to the fact that the 50 μm thick films were processed at lower MD extension rates (lower draw-down ratio) than their 25 μm thick counterparts.

Patel et al. [17] investigated the influence of process conditions on the blown film properties of a commercial LLDPE resin. In their study, they found no systematic correlation, whatsoever, between tear resistance and process conditions. We calculated the MD extension rate imparted to their films based on the process conditions provided in their article. This allowed us to consider the extension rate dependence of tear resistance exhibited by their blown films; these data are also plotted in Fig. 2. Note that only those samples processed using a die land length of 1 in. are considered here to avoid any influences exerted by factors other than the extensional stresses along the bubble. The trend of decreasing MD tear with increasing MD extension rate appears to hold good for their samples as well. In summary, low-MD extension rates and small process Deborah numbers tends to yield blown films with higher Elmendorf MD tear resistance.

In Fig. 3, the TD tear resistance of all the blown films considered in Fig. 2 are plotted versus the MD extension rate as determined using Eq. (3). Similar to the MD tear results, the TD tear resistance is observed to be a strong function of the process conditions employed. Specifically, for all the LLDPEs considered, the blown film TD tear resistance is observed to increase systematically with increasing MD extension rate. Consequently, while low Deborah numbers were observed to favor high MD tear, high Deborah numbers favor high TD tear.

4.3. Orientation characteristics of LLDPE blown films

In order to understand the structural features that contribute to the Elmendorf tear resistance of LLDPE blown films, it is important to characterize their orientation features. The orientation features of various polyethylene blown films have been characterized previously [9,18–30]

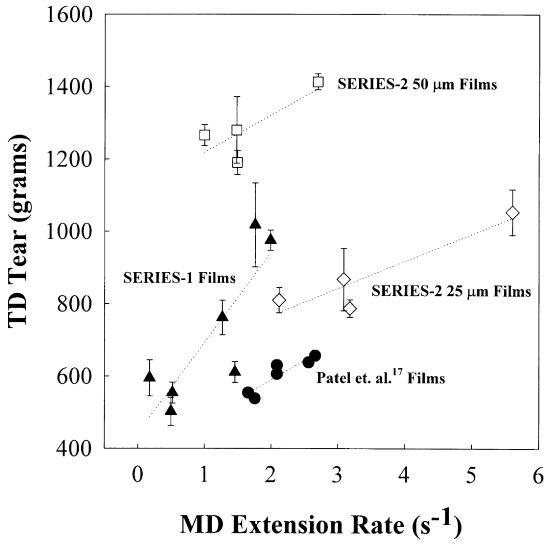

Fig. 3. LLDPE blown film TD tear resistance plotted as a function of MD extension rate for SERIES-1 and SERIES-2 films.

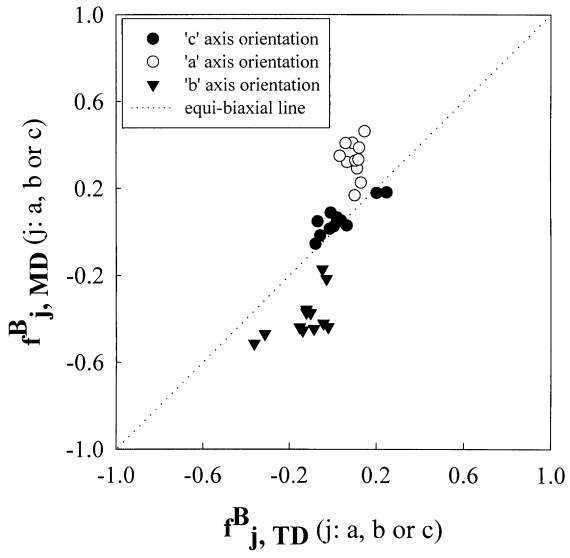

Fig. 4. Biaxial orientation factors of the crystalline phase plotted in terms of the White–Spruiell diagram for SERIES-3 LLDPE blown films.

and the results have typically been interpreted in terms of the morphological models proposed by Keller and co-workers [31,32]. In this study, all the orientation features are described in terms of the White–Spruiell biaxial orientation factors [9,18,19]. The biaxial orientation factors of the crystalline phase in all the LLDPE blown films were estimated according to procedures described previously [9]. The orientation factors of the non-crystalline chain segments in the blown films were estimated using in-plane and out-of-plane birefringence measurements in conjunction with the orientation factors of the crystalline phase using equations presented and applied previously [18,19]. The biaxial orientation factors of the crystalline phase (*a*, *b* and *c* unit cell axes) in SERIES-3 blown films are plotted in the form of the White–Spruiell [9,18,19] orientation diagram in Fig. 4 (it is cautioned that the typical standard deviation in these numbers are of the order ^ 0.03). Essentially in Fig. 4, the White–Spruiell biaxial orientation factor of the crystal unit cell axes along the film MD are plotted versus their counterparts along the film TD. The dotted line in Fig. 4 represents equi-biaxial orientation along the plane of the film. Examination of the data indicates that all SERIES-3 blown films display preferential orientation of the *a*-axis in the crystalline phase along the film MD. This is consistent with previous measurements (using WAXS) of crystalline phase orientation in LLDPE and LDPE blown films [9,18,19]. In fact, preferential orientation of the *a*-axis (relative to *c*-axis) along the MD (Keller–Machin I "row" structure) has been observed in most polyethylene blown films barring some HDPE films. Therefore, our observations are largely consistent with expectations based on prior orientation studies of LLDPE blown films [18–30].

In the SERIES-3 blown films, while the *a*-axis displays significant orientation in the plane of the film and especially along the MD, the *c*-axis is not as strongly oriented and displays close to equi-biaxial orientation in the plane of the film. The *b*-axis (lamellar growth axis), however, displays a strong orientation orthogonal to the film MD. In fact, the *b*-axis appears to be located largely in the film TD-normal plane with a stronger orientation along the film normal. Orientation of the *b*-axis in SERIES-3 films is also consistent with prior measurements on similar films [9,18,19,21–23].

Fig. 5 shows WAXS patterns for three of the SERIES-3 blown films, namely, LLDPE-1, LLDPE-5 and LLDPE-7. Also indicated in Fig. 5 are the biaxial orientation factors of the unit cell *a*-axis along the MD as estimated using previously developed methodology [9]. Before proceeding further, it is important to realize that polyethylene crystallizes in the form of orthorhombic unit cells. In these WAXS patterns, reflections (Debye–Scherer rings) from the (110) and (200) crystal planes are evident. The intensity of the (200) reflection is concentrated along the meridional plane for all three films. Further, the intensity of the (110) reflection has a maximum away from the equitorial plane. These observations indicate preferential orientation of the *a*-axis along the film MD in these films. Also, based on the azimuthal dependence of the intensity of the (200) reflection, the degree of *a*-axis orientation along the MD in these films are observed to be in the order LLDPE-7 > LLDPE-1 > LLDPE-5. This trend, based on the azimuthal dependence of the (200) reflection is consistent with our quantitative estimations [9]. Further, these WAXS patterns confirm that the LLDPE blown films considered here reveal preferential orientation of the unit cell *a*-axis along the film MD (Keller–Machin I "row" structure).

We also note that the extent of *a*-axis orientation along the plane of the film is a function of the molecular characteristics of the resin. In general, within the resin set considered here, LLDPEs based on Ziegler–Natta catalysts and

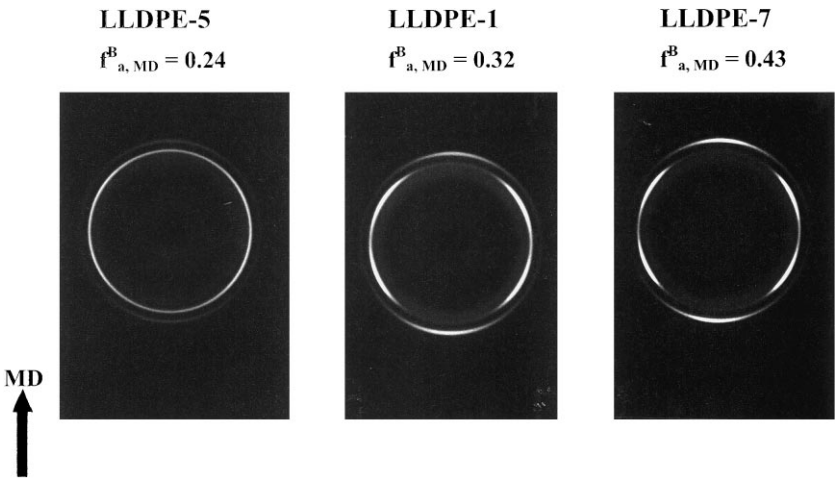

Fig. 5. Wide-angle diffraction patterns for three representative SERIES-3 LLDPE blown films (LLDPE-5, LLDPE-1, and LLDPE-7).

chromium oxide catalysts tend to display higher degrees of crystalline orientation relative to the LLDPEs based on metallocene catalysts. This is possibly due to the differences in the manner in which these polymers crystallize under the influence of stresses. Very little information, if any, is available on flow-induced crystallization of such polymers to postulate as to why metallocene catalyzed LLDPEs display lower levels of crystalline orientation. However, one does note (from Table 1) that the metallocene catalyzed LLDPEs considered here are of lower molecular weight (lower M_w and substantially lower M_z) which is also reflected in their shorter melt-relaxation times. Therefore, it is possible that the greater number of high molecular weight nucleation sites in chromium oxide and Ziegler–Natta catalyzed LLDPEs (relative to metallocene catalyzed LLDPEs) aid in attaining higher degrees of crystalline orientation in the blown film process [32].

Using the calculated orientation factors of the crystalline phase in combination with the measured birefringence (in-plane and out-of-plane) in these blown films, the biaxial orientation factors of the non-crystalline chain segments were calculated [18,19]. In these calculations, the weight fraction crystallinity was estimated from density measurements using a two-phase (crystalline and amorphous) model. Further, the following intrinsic birefringences for the amorphous and crystalline phases were employed: $\Delta^0_{am} = 0.058$; $\Delta^0_{cb} = 0.056$; $\Delta^0_{ab} = -0.005$ [19]. In doing so, we observed that the non-crystalline chain segments are oriented to a reasonable extent and are located largely in the plane of the film. Further, the degree of orientation in the non-crystalline phase for the above blown films was observed to be lower than that of their crystalline counterparts.

Transmission electron microscopy (TEM) is an efficient tool to examine lamellar morphology and organization in semi-crystalline polymers. In Fig. 6, TEM images of three representative SERIES-3 blown films are shown (LLDPE-5, LLDPE-1, and LLDPE-7). In these micrographs, the machine direction is approximately indicated by the white arrow marks. The long axes of the lamellae and the inter-lamellar non-crystalline phase appear as alternating white and dark regions in Fig. 6. The micrographs also indicate that the lamellar long axis is largely orthogonal to the film MD. The lamellar orientation as observed in the TEM images is consistent with the orientation estimates for the *b*-axis. These results are also consistent with prior observations of crystallization under the influence of stresses wherein lamellar growth has always been observed to occur orthogonal to the direction of the principal stresses [31,32]. Substantial curvature of the lamellae is also noticeable in some films. Specifically, lamellar curvature

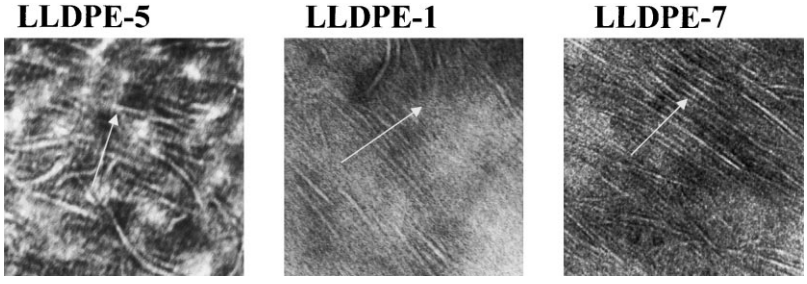

Fig. 6. Transmission electron micrographs showing the lamellar morphology of three representative SERIES-3 LLDPE blown films (LLDPE-5, LLDPE-1, and LLDPE-7). The magnification in these images is approximately 10^5.

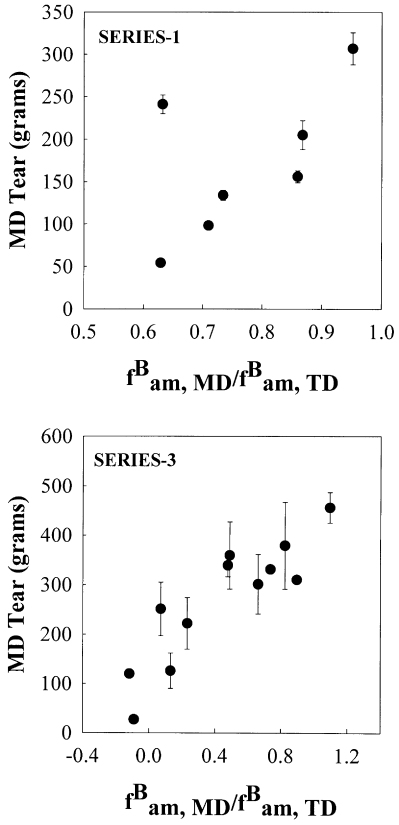

Fig. 7. Blown film MD tear resistance plotted as a function of $f^{B}_{am,MD}/f^{B}_{am,TD}$ for SERIES-1 and SERIES-3 LLDPE blown films.

appears to be quite significant in metallocene catalyzed LLDPE blown films and least evident in chromium oxide catalyzed LLDPE blown films, with the Ziegler–Natta catalyzed LLDPE films revealing lamellar character that is somewhat intermediate. One also observes that the metallocene catalyzed LLDPE films reveal somewhat shorter lamellae as well in comparison to those of the chromium oxide and Ziegler–Natta catalyzed LLDPE films. These features are attributable to the molecular architecture of the different polymers and how they crystallize under the influence of stresses. In general, the LLDPE resins with the shortest relaxation times and lowest molecular weights tend to display greater degrees of lamellar curvature in the blown films considered here.

Although not shown here (for the sake of brevity), the orientation and morphological characteristics of SERIES-1 and SERIES-2 blown films are very similar to those of SERIES-3 films described above. In summary, the LLDPE blown film microstructure can be described as a parallel array of lamellae with their long axes along the TD-normal plane. Possibly, some degree of lamellar twisting (or tilting) has resulted in the crystal *a*-axis being oriented preferentially along the film MD. Such a morphology is typically referred to as the Keller–Machin "row" structure [18,19,31,32].

4.4. Influence of orientation on blown film tear resistance

In Fig. 7, the MD tear resistance of SERIES-1 and SERIES-3 blown films are plotted as a function of a measure of anisotropy in the orientation of the non-crystalline chain segments within the plane of the film. Specifically, the *x*-axis in Fig. 7 is the biaxial orientation factor of the non-crystalline chains along the MD divided by its counterpart along the TD of the blown film ($f^{B}_{am,MD}/f^{B}_{am,TD}$). When $f^{B}_{am,MD}/f^{B}_{am,TD}$ is equal to "one", the non-crystalline chains, on average, are oriented equi-biaxially in the plane of the film. Substantial deviation from one is an indication of higher degrees of uniaxial orientation of the non-crystalline chain segments relative to equi-biaxial orientation. In Fig. 7, we observe that the films with the highest MD tear resistance are those in which $f^{B}_{am,MD}/f^{B}_{am,TD}$ is closest to one. This trend of increasing MD tear as $f^{B}_{am,MD}/f^{B}_{am,TD}$ approaches one holds true for both SERIES-1 (single resin and various process conditions) and SERIES-3 (various LLDPE resins and constant process conditions) blown films. Although not shown here, similar trends were observed for the SERIES-2 films as well. Therefore, closer the non-crystalline chain segments are to equi-biaxial orientation in the plane of the film, higher is the resistance to tear propagation along the film MD.

The *b*-axis in polyethylene is known to be along the lamellar growth (lamellar long axis) direction. Therefore, orientation of the *b*-axis can be used as an indicator of the lamellar long axis orientation. From before, we know that the *b*-axis in the LLDPE blown films investigated is located along the TD-normal plane with a preferential orientation along the film normal. In Fig. 8, the TD tear resistance of SERIES-1 and SERIES-3 blown films are plotted as a function of a measure of anisotropy in the orientation of the unit cell *b*-axis along the plane of the film. In other words, the *x*-axis in Fig. 8 is the biaxial orientation factor of the crystalline *b*-axis along the MD minus its counterpart along the TD ($f^{B}_{b,MD} - f^{B}_{b,TD}$) of the blown film. A low value of ($f^{B}_{b,MD} - f^{B}_{b,TD}$) indicates that the lamellar long axis is aligned closer to the film TD. Further, a low value of ($f^{B}_{b,MD} - f^{B}_{b,TD}$) also indicates lower degrees of lamellar curvature. The trend evident in Fig. 8 (for SERIES-1 and SERIES-3 blown films) indicates that a small value of ($f^{B}_{b,MD} - f^{B}_{b,TD}$) translates to higher resistance to tear propagation along the film TD. Similar trends (not shown here for purposes of brevity) were evident for the SERIES-2 blown films as well. This result indicates that relatively straight (lower degrees of curvature) lamellae oriented closer to the film TD enhances resistance to tear propagation along the film TD.

At this point, it is important to realize that despite some scatter in the trends evident in Figs. 7 and 8, these observations are unique and important because of the broad spectrum of LLDPE resins and process conditions considered in this work. Despite structural characterization of LLDPE blown films in the past, NO systematic trends or correlations have been published that describe tear performance in terms of

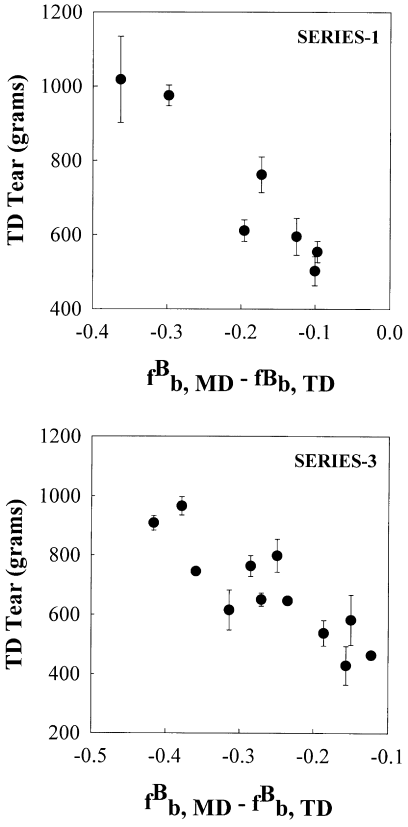

Fig. 8. Blown film TD tear resistance plotted as a function of $f^B_{b,MD} - f^B_{b,TD}$ for SERIES-1 and SERIES-3 LLDPE blown films.

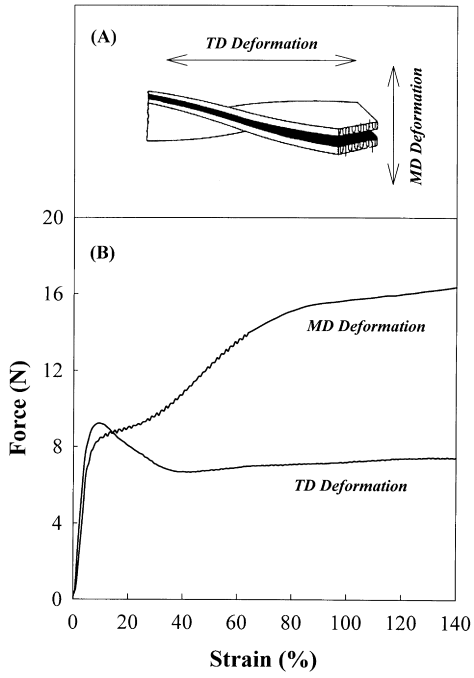

Fig. 9. (A) Schematic of LLDPE blown film lamellar morphology. (B) Tensile stress–strain curve along the MD and TD of a representative SERIES-3 LLDPE blown film.

molecular orientation. Consequently, we believe that these results are unique and deserve further attention.

5. Discussion

In this section, based on the observed dependence of MD and TD tear on aspects of molecular orientation, an attempt will be made to associate blown film tear propagation with appropriate microstructural deformation mechanisms on the crystalline lamellar size-scales. In order to do so, it is important to understand the dynamics of the Elmendorf tear test. The Elmendorf tear test (ASTM D-1922) is a measure of resistance to propagation of a tear, which in turn is initiated via a pre-introduced slit in the specimen. Also, and perhaps most importantly, substantial stretching of the film specimen is evident prior to propagation of the tear in an Elmendorf tear test. In other words, the contour length of the torn edge of the film specimen (after the tear test) is substantially greater than the initial length of the film specimen. In fact, even the ASTM standard for tear testing warns the users of specimen stretching during the test. Consequently, in the following structural interpretations of tear propagation during an Elmendorf tear test, this stretching phenomenon will be important to keep in mind. The arguments presented hereafter assume that specimen stretching and the associated microstructural deformations are responsible for distinguishing LLDPE blown films of high and low tear resistance. Further, while our intention is to focus on the possible microstructural deformations that distinguish films of varying Elmendorf tear resistance, it is not our intent here to list all possible molecular rearrangements that could occur during the Elmendorf tear test.

It is important to re-iterate that we intend to borrow the wealth of knowledge accumulated on the solid state processing of polymers and apply those principles to explain tear propagation in LLDPE blown films. After all, the Elmendorf tear test involves solid state deformation of the film specimen with substantial stretching occurring prior to tear propagation. Because we assume that specimen stretching plays an important role in distinguishing LLDPE blown film Elmendorf tear resistance, let us consider tensile deformation (as in stretching) of the subject films in terms of microstructural deformations. In Fig. 9A, based on the orientation and morphological results, a simplistic schematic of the lamellar morphology of LLDPE blown films is shown. In Fig. 9B, the tensile stress–strain curve of a representative LLDPE blown film is shown along both its MD and TD. When a lamellar structure such as the one shown in Fig. 9A is deformed in the tensile mode, the resistance offered by the structure will depend strongly on the direction of the applied load. For instance, if the forces are applied along the film MD with the long axis of the lamellae being orthogonal to MD, deformation of the “soft”, non-crystalline phase is readily achieved as the crystalline lamellae and the interlamellar amorphous components tend to

deform in a constant-stress mode [3,7,8,33–36]. Such a deformation mode is similar to the inhomogeneous deformation of a spherulite along its equatorial region [3]. The non-crystalline phase tends to deform predominantly via interlamellar shear and lamellar separation along this direction. These deformation mechanisms have been identified and believed to be dominant during the initial stages of tensile deformation along the MD of uniaxially oriented polyethylene [7,8,35,36]. At higher strain levels, the onset of plastic deformation possibly proceeds via crystallographic slip followed by break-up of the lamellar structures leading to catastrophic failure of the material. Formation of extended chain crystals has also been observed prior to material fracture/failure [3,7,8,33–36].

Let us now consider tensile deformation along the TD of blown films. In this mode, the long axis of the lamellae is located in the TD–ND plane, with the forces being applied along the TD (see Fig. 9A). Consequently, the stresses are distributed primarily along the long axis of the rigid crystalline lamellae due to the approximately constant strains imposed on the crystalline and non-crystalline phases [3,7,8,33–36]. Such a deformation mode is similar to the inhomogeneous deformation of a spherulite along its polar region [3]. In this circumstance, deformation of the interlamellar non-crystalline phase and plastic deformation via crystallographic slip are severely hindered due to the direction of chain folding (within the lamellar crystals) relative to the direction of the applied load [34,35]. In uniaxially oriented polyethylene, deformation along the TD involved very little contribution from the non-crystalline phase prior to yield; the yield in this case appeared to correspond to the onset of chain pull-out along the lamellar long axis followed by alignment of the chains along the direction of the applied load [34,35].

On heating blown and cast films to temperatures close to their melting point, substantial shrinkage is observed along the film MD while shrinkage is minimal (non-measurable) along the TD [17]. The shrinkage along the MD is presumably due to relaxation of the extended conformation of the non-crystalline chains in the blown film. This orientation relaxation in the interlamellar region does not contribute to macroscopic shrinkage along the TD, possibly due to the orientation of the rigid lamellae along the TD-normal plane. This is another indication that deformation along the MD involves the non-crystalline phase while deformation along the TD is relatively constrained by the long axis of the lamellae (negligible shrinkage). In a separate process study [17], the MD tear resistance of various LLDPE blown films appeared to correlate reasonably well with measured shrinkage along the MD. This suggests that deformations in the interlamellar non-crystalline phase perhaps contribute in some manner to the measured resistance to tear propagation along the film MD. In the LLDPE blown films considered here (from Fig. 7), the resistance to MD tear propagation was observed to be higher when the non-crystalline chain segments were oriented equi-biaxially in the plane of the film (aligned at approximately equal angles with respect to the MD and TD). Interlamellar shear deformation is more likely to dominate in cases when the non-crystalline chains and especially the taut tie-molecules are oriented equi-biaxially in the plane of the film relative to cases where the non-crystalline chains are oriented uniaxially [7,8]. Further, SEM examinations of tear propagation along the MD of HDPE blown films indicate highly localized yielding at the tear propagation tip with evidence of lamellar rotation [37]. All of the above results appear to suggest that interlamellar shear deformation could play an important role in distinguishing LLDPE blown films of high and low MD tear resistance.

We have also observed that LLDPE films blown at low MD extension rates (low Deborah numbers) tend to offer greater resistance to tear propagation along the MD (Fig. 2). As the polymer molecules exit the film die, the extensional forces applied will tend to orient them along the stresses. Relaxation of the extended conformation of these chains will simultaneously be in competition with their orientation prior to the crystallization process. Consequently, at high MD extension rates, a greater number of molecules will be oriented along the MD prior to the onset of crystallization. This, evidently, is detrimental from a MD tear performance perspective (Fig. 2). Without a clear stress-induced crystallization model, it is difficult to correlate this extension rate dependence with the morphological dependence and the possible role played by interlamellar shear deformation. However, at higher MD extension rates with the molecules aligned to a greater extent along the MD prior to the onset of crystallization, it is reasonable to assume that the non-crystalline phase in the final film, on average, will tend to be oriented more uniaxially relative to equi-biaxial in the plane of the film. This, in turn, will inhibit interlamellar deformations to some extent thus expediting the onset of plastic deformation (presumably, via crystallographic slip) to relatively lower strains. This could perhaps lower the resistance to tear propagation along the MD of the blown film. Thus, the observed extension rate dependence appears to be consistent with the hypothesis that interlamellar deformations are important during tear propagation along the MD of LLDPE blown films.

In Fig. 8, the TD tear of the LLDPE blown films was observed to be higher when the long axis of the lamellae are minimally curved and oriented closer towards the film TD. Closer the long axis of the lamellae is to TD and lower the degree of lamellar curvature, greater will the stresses borne by the lamellae itself be; this, in turn, results in higher resistance to tear propagation along the TD. Therefore, we observe that lamellar orientation and curvature are critical factors in distinguishing the TD tear resistance of LLDPE blown films. Further, in Fig. 3, the TD tear of LLDPE blown films was observed to depend strongly on the MD extension rate imposed in the process. Specifically, higher MD extension rates were observed to favor TD tear resistance. At higher extension rates, with shorter structural reorganization

times available, lower degrees of lamellar curvature is anticipated. The orientation results indicate that lower degrees of curvature indeed favor TD tear resistance. Thus, the observed dependence of TD tear on MD extension rate appears to be consistent with the orientation results which indicate that lamellar orientation and curvature are critical factors in distinguishing the TD tear resistance of LLDPE blown films. Consequently, plastic deformation by chain pull-out along the lamellar long axis and their subsequent alignment along the TD is suggested to be the distinguishing microstructural deformation mechanism that is operative during tear propagation along the TD of LLDPE blown films.

Let us now examine the tensile stress–strain traces for a representative LLDPE blown film along its MD and TD as shown in Fig. 9B. The qualitative characteristics depicted in the stress–strain curve in Fig. 9B were evident in all the LLDPE blown films investigated here; the detailed tensile properties will be summarized in a separate report [38]. While the tensile stress–strain curves along the MD do not reveal a distinct yield point (relative maxima in stress), the traces appear to indicate the existence of two yield points, a phenomenon noted previously in polyethylene blown films [39] and isotropic specimens [33,34]. This has typically been referred to as "double-yielding". This double-yielding phenomenon has been attributed to deformations in the interlamellar regions [33–36]. Thus, the double-yielding characteristics observed along the MD of LLDPE blown films appear to add credence to the suggestion that interlamellar deformations play an important role in distinguishing LLDPE blown films of high and low MD tear resistance.

Contrary to tensile deformation along the MD, a single distinct yield point is observed along the TD. It is also evident that the yield point along the TD occurs at much lower strains than along the MD. This is due to the fact that initial deformation along the TD is relatively constrained by the long axis of the crystalline lamellae. Thus, the substantially lower yield strain along the TD (relative to MD) of the blown films appear to add credence to the earlier suggestion that the stresses borne along the lamellar long axis play an important role in distinguishing LLDPE blown films of high and low TD tear resistance.

Excellent correlation between the Elmendorf tear properties of LLDPE blown films and their tensile yield characteristics have been observed [38]. This adds substantial credibility to our earlier hypotheses that specimen stretching plays a significant role in Elmendorf tear tests and further supports the proposed structural features and microstructural deformation mechanisms that are deemed critical in distinguishing LLDPE blown film tear resistance performance.

In considering microstructural deformation mechanisms that are possibly operative during tear propagation, it was suggested that interlamellar deformations and plastic deformation via chain pullout (along lamellar long axis) were the *distinguishing* mechanisms responsible for the Elmendorf tear resistance along the MD and TD of LLDPE blown films, respectively. In considering the above mechanisms, some simplifying assumptions have been made. First, stretching of the film specimen and its associated microstructural deformations were considered to be significant in an Elmendorf tear test; recently, this assumption was shown to be reasonably valid [38]. Second, in considering possible microstructural deformation mechanisms responsible for MD tear propagation, contributions from various other deformations and defects were ignored mainly due to our inability to characterize them experimentally.

In summary, this work has explored the effects of orientation in the crystalline and non-crystalline phases on tear resistance along the MD and TD of LLDPE blown films. Considering the commercial significance of Elmendorf tear resistance results and the lack of published knowledge with regards to how structure influences tear propagation, these results appear to be quite significant. Nevertheless, the observed orientation results may provide only one part of the ultimate answer with regard to polyethylene blown film tear resistance.

6. Conclusions

Investigation of the crystalline phase orientation in the LLDPE blown films indicated preferential orientation of the unit cell *a*-axis along the film MD (Keller–Machin-I "row" structure) with the lamellar long axis located along the TD-normal plane in all films. Further microscopic examinations indicated that the lamellar long axis was indeed orthogonal to the film MD. Also, substantial curvature of the lamellae was evident in some films; the degree of lamellar curvature was a function of the resin and processing characteristics. Orientation in the non-crystalline phase was observed to be substantial, although the degree of orientation was not as high as in the crystalline phase. Essentially, the LLDPE blown film microstructure can be described as a parallel array of lamellae with their long axes along the TD-normal plane. Possibly, some degree of lamellar twisting (or tilting) has resulted in the crystal *a*-axis being oriented preferentially along the film MD. These observations are consistent with prior orientation studies on similar films [18–30] and are typically interpreted in terms of the Keller–Machin "row" structure [31,32].

The Elmendorf tear performance of LLDPE blown films was observed to be dependent on the process extension rate imposed along the MD. Lower MD extension rates (low Deborah numbers) were observed to favor MD tear performance, while higher MD extension rates (high Deborah numbers) were observed to favor TD tear performance.

Based on the dynamics of the Elmendorf tear test, it was assumed that specimen stretching plays an important role in distinguishing the tear resistance of LLDPE blown films.

Investigation of the orientation (crystalline and non-crystalline) characteristics of various LLDPE blown films indicated that the MD tear resistance was higher when the non-crystalline chains, on average, were closer to equi-biaxial in the plane of the film. These observations indicated that interlamellar shear deformation could play an important role in distinguishing LLDPE blown films of high and low MD tear resistance. It was suggested that interlamellar shear deformation, possibly accompanied by lamellar rotation and separation could delay the onset of plastic deformation via crystallographic slip thus enhancing the resistance to tear propagation along the film machine direction.

Investigation of the lamellar orientation in various LLDPE blown films indicated that the TD tear resistance was high when the crystalline lamellae were relatively straight (minimal curvature) and oriented closer to the film TD. These investigations indicated that the stresses borne along the long axis of the lamellae during propagation of a tear along the film TD may distinguish LLDPE blown films of high and low TD tear resistance. Consequently, plastic deformation by chain pull-out (unfolding) along the lamellar long axis and their subsequent alignment along the TD was suggested to be the distinguishing microstructural deformation mechanism that could be operative during tear propagation along the TD of LLDPE blown films.

The proposed microstructural deformation mechanisms deemed to discern the Elmendorf tear resistance of LLDPE blown films were observed to be consistent with those that are operative during the controlled tensile stretching of oriented polyethylene specimens. Further, these results were also observed to be consistent with the dependence of tear resistance on the imposed extension rate in the blown film process. Thus, despite certain simplifying assumptions, we believe that significant insights have been gained not only on the dependence of tear resistance on molecular orientation characteristics but also on possible microstructural deformation mechanisms that could be operative during tear propagation in an Elmendorf tear test.

Acknowledgements

The encouragement and assistance offered by Prof. Garth Wilkes (Virginia Tech) and Prof. Stephen Cheng (University of Akron) is greatly appreciated. The WAXS patterns and TEM images were obtained through Prof. Garth Wilkes. Jerry Stark and David Higbee were responsible for all the film blowing and testing. Dr David Rohlfing and Mike Hicks are appreciated for rheological characterization of the resins used. Dr Tim Johnson and Deloris Henson are acknowledged for SEC data. Drs Jay Janzen and Mark Lamborn are acknowledged for several useful discussions. Don Renfro performed all the IR absorption experiments. John Jackson from the Metricon Corporation is acknowledged for his assistance with the Metricon Prism Coupler and birefringence measurements. Useful comments from one of the reviewers are greatly appreciated. Finally, Phillips Petroleum Company is acknowledged for permission to publish this work.

References

[1] Ross JF, MacAdams JL. The polymeric materials encyclopedia. New York: CRC Press, 1996 (Polyethylene ‘Commercial’, p. 5953–65).
[2] Osborn KR, Jenkins WA. Plastic films—technology and packaging applications. Lancaster: Technomic, 1992.
[3] Lin L, Argon AS. Journal of Material Science 1994;29:294.
[4] Porter RS, Wang LH. Journal of Macromolecular Science: Macromolecular Chemical Physics 1995;C35:63.
[5] Ward IM. Structure and properties of oriented polymers. 2nd ed.. New York: Chapman and Hall, 1997.
[6] Peterlin A. Colloid and Polymer Science 1987;265:357.
[7] Keller A, Pope DP. Journal of Material Science 1971;6:453.
[8] Pope DP, Keller A. Journal of Polymer Science: Polymer Physics Edition 1975;13:533.
[9] Krishnaswamy RK. Journal of Polymer Science: Polymer Physics Edition 2000;38:182.
[10] Janzen J, Rohlfing DC, Hicks MJ. Journal of Rheology 1999 (in press).
[11] Arnett RL, Thomas CP. Journal of Physical Chemistry 1980;84:649.
[12] Janzen J, Colby RH. Journal of Molecular Structure 1999;485-486:569.
[13] Dealy JM, Wissbrun KF. Melt rheology and its role in plastics processing. New York: Chapman and Hall, 1995.
[14] Sukhadia AM. Journal of Plastic Film and Sheeting 1994;10:213.
[15] Ghaneh-Fard A, Carreau PJ, Lafleur PG. Polymer Engineering and Science 1997;37:1148.
[16] Ghaneh-Fard A, Carreau PJ, Lafleur PG. International Polymer Processing 1997;12:136.
[17] Patel RM, Butler TI, Walton KL, Knight GW. Polymer Engineering and Science 1994;34:1506.
[18] White JL, Cakmak M. Advances in Polymer Technology 1988;8:27.
[19] Pazur RJ, Prudhomme RE. Macromolecules 1996;29:119.
[20] Holmes DR, Palmer RP. Journal of Polymer Science 1958;31:345.
[21] Maddams WF, Preedy JE. Journal of Applied Polymer Science 1978;22:2721.
[22] Maddams WF, Preedy JE. Journal of Applied Polymer Science 1978;22:2739.
[23] Maddams WF, Preedy JE. Journal of Applied Polymer Science 1978;22:2759.
[24] Choi K, Spruiell JE, White JL. Journal of Polymer Science: Polymer Physics Edition 1982;20:27.
[25] Kwack TH, Han CD. Journal of Applied Polymer Science 1988;35:363.
[26] Kalyon DM, Moy FH. Polymer Engineering and Science 1988;28:1551.
[27] Kissin YV. Journal of Polymer Science: Polymer Physics Edition 1992;30:1165.
[28] van Gurp M, Kip BJ, van Heel JPC, de Boer S. Journal of Plastic and Film Sheeting 1994;10:156.
[29] Simpson DM, Harrison IR. Journal of Plastic and Film Sheeting 1994;10:302.
[30] Fruitwala H, Shirodkar P, Nelson PJ, Schregenberger SD. Journal of Plastic and Film Sheeting 1995;11:298.
[31] Keller A, Machin MJ. Journal of Macromolecular Science 1967;B1:41.

[32] Keller A, Kolnaar HWH. Material Science and Technology 1997;18:189.
[33] Brooks NW, Duckett RA, Ward IM. Polymer 1992;22:1975.
[34] Brooks NW, Unwin AP, Duckett RA, Ward IM. Journal of Macromolecular Science: Physics Edition 1995;34:29.
[35] Zhou H, Wilkes GL. Journal of Material Science 1998;33:287.
[36] Butler MF, Donald AM. Macromolecules 1998;31:6234.
[37] Sherman ES. Polymer Engineering and Science 1984;24:895.
[38] Krishnaswamy RK, Lamborn MJ. Polymer Engineering and Science. Submitted for publication.
[39] Feijoo JL, Sanchez JJ, Muller AJ. Polymer Bulletin 1997;39:125.